Vol. 14(4), pp. 97-109, October-December, 2022
DOI: 10.5897/IJWREE2022.1037
Article Number: 24CD44C69833
ISSN: 2141-6613

http://www.academicjournals.org/IJWREE

ACADEMIC JOURNALS
expand your knowledge

International Journal of Water Resources and Environmental Engineering

Full Length Research Paper

Investigation of voltage storage capacity for the variation of electrode materials in microbial fuel cells with experimentation and mathematical modelling

Al-Mustasin Abir Hossain[1]*, Nahian Masud[2], Subrato Roy[3] and Mohammad Ali[2]

[1]Department of Mechanical Engineering, The University of Texas at Dallas, Texas, United States.
[2]Department of Mechanical Engineering, Bangladesh University of Engineering and Technology (BUET), Dhaka, Bangladesh.
[3]Department of Mechanical Engineering, School of Engineering and Computer Science (ENCS), Washington State University, Vancouver, United States.

Received 2 June, 2022; Accepted 4 October, 2022

Microbial fuel cells (MFCs) are considered as one of the best prospective natural resources to be discovered on the way to reduce the dependence on fossil fuel-based electricity generation. However, low power generations from MFCs, expensive electrode materials, and the inability to scale-ups MFCs to industrially relevant capacities have made the usage of MFC even worse. The utilization of MFCs in the area of electro-chemistry and thermal science can be very promising in energy storage aspects. In this current study, we studied various combinations of electrode materials and processes that can be applied to construct economical MFCs on small scale. To figure out the best suited MFC setup, MFC systems are prepared using different electrode materials and impacts of these materials on voltage generation are investigated. The cells are observed for 10 h, and voltage generation is witnessed by natural chemical reaction. Then, voltage, current, and power density curves are generated. Next, a pseudo-two-dimensional (2D) physics-based mathematical full cell model is developed to investigate the best suited MFC as a potential energy storage device. It is observed that the numerical results generated from the model are in good agreement with those obtained from the experimental analyses. Hence, the model should be able to predict the better performing anode and cathode materials to build microbial fuel cells having a maximum amount of voltage storage capacity in a specific period. Details of this work will provide more useful information on the concept of MFC and design guidelines for several applications such as energy storage and transformation.

Key words: Bacteria, electro-chemistry, physics-based, power, energy storage device, electrodes.

INTRODUCTION

Harvesting energy from fossil fuels is a traditional way to meet up the demand of energy alternatively by only increasing the efficiency; this might not be possible to keep living on indefinitely (Oliveira et al., 2013). Therefore, improvement in energy conservation and efficiency are needed through newer technology to gradual replace

*Corresponding author. E-mail: al-mustasin.hossain@utdallas.edu

fossil energy by renewable energy (Oliveira et al., 2013). In this regard, Microbial fuel cell (MFC) constitutes a promising technology for sustainable production of alternative energy and treatment of wastes such as the spent liquor of dark fermentation (Hernández-Flores et al., 2015). The interest towards MFC as renewable energy increases because they can produce electricity directly from the waste generated from daily activities and can degrade toxic compounds and pollutants. In wastewater treatment plants, waste-water can be used to produce electricity by MFCs (Pinto et al., 2010). Sustainable energy productions from renewable sources can reduce the emission of CO_2 (Min et al., 2005). In an MFC, the chemical energy is converted to electrical energy with the help of microorganism. In MFCs, oxidation is used as the means of generation of electron and is transferred directly to an anode or redox mediator separator. On the other hand, electron flux is moved to cathode. Most MFCs use an organic electron donor that is oxidized to produce carbon-di-oxide (CO_2), protons, and electrons. Other electron donors have been reported, such as sulphur compounds or hydrogen. The cathode reaction uses a variety of electron acceptors, most often oxygen. Few other electron acceptors studied in the past include metal recovery by reduction (Lu et al., 2015) water to hydrogen (Oh and Logan, 2015) nitrate reduction, and sulphate reduction.

There are many factors which affect the electric energy production in an MFC. Some of the most important ones are the nature of the bio-catalysts, the type and materials of electrodes, electrode catalysts, cell configuration, and architectural design (Belleville et al., 2011; Logan and Regan, 2006; Valdez-Vazquez et al., 2006). A downside of using MFC in practical scenarios is the ohmic overpotential which is also known as internal resistance. It includes both the resistance to the flow of electrons through the electrodes and interconnections and the resistance to the flow of ions through the membrane and the anodic and cathodic electrolytes (only anodic electrolyte in a single chamber MFC). This internal resistance depends on some factors such as the surface area of electrodes, distance between electrodes, anodic material conductivity, the presence or absence of membrane, the type of electrolyte(s) Belleville et al. (2011) carried out an investigation of the limitations of nitrogen on the performance of MFC. Li et al. (2009) investigated the effects of configurations, electrolyte solutions and electrode materials on power generations. Among all these variable parameters, electrode material can have a great influence on the reduction of internal resistance. For example, to use a material as anode, it must have few key characteristics such as high electrical conductivity, strong biocompatibility, chemical stability and anti-corrosion, large surface area and appropriate mechanical strength and toughness.

There are some past studies on the properties of electrode materials for MFC. One of the key focuses is to replace platinum as an electrode material towards the carbon materials and non-corrosive materials. The high cost of platinum plays an important role in this shifting. Besides, platinum shows antimicrobial properties leading to the inhibition of the *E. coli* division, due to products produced (cisplatin) from a platinum electrode during electrolysis (Yang, 2009; Ghasemi et al., 2013; Rosenberg et al., 1965). The topography of electrode material can also have key impacts on power generation. A high surface area is desirable, and a relatively rough surface is thought to be an ideal surface property in a MFC configuration, as it helps with the retention of the bacteria to the surface (Wei et al., 2011). Surface roughness and area of the electrode materials has also been shown to play an important role in the generation of electricity (Walter et al., 2016). Carbon cloth has been a popular electrode material of choice for MFCs; this is due to its reported useful conductivity, stability, commercial availability, and relatively inexpensive cost, in comparison to other carbon-based electrode materials (Liu and Logan, 2004; Liu et al., 2012). It consists of long individual carbon fibres, between 5 to 7 µm in diameter and is produced via the thermal decomposition of acrylic. These individual fibres are joined together as a bundle and are then weaved together to produce the carbon cloth (Cœuret et al., 2002). Another carbon-based electrode useable in MFC is carbon felt. One study has compared the efficacy of carbon felt anodes, using bacteria isolated from sludge from a domestic wastewater plant (Cœuret et al., 2002). The results showed that under anaerobic conditions, a maximum power density of 7.07 ± 0.45 mW/m^2 was produced (Chen et al., 2013). In our case we used carbon cylinder to make the MFC cell cost effective and simpler.

Graphite has exceptional electrochemical properties. An abundance of a monoculture biofilm (*E. coli*) can be seen from SEM image, adhered to a graphitic electrode surface as the material has bio-compatibility. A study by some researchers demonstrated that increasing the graphite surface area available for microbial colonization increased power outputs (Chaudhuri and Lovley 2003). Another interesting choice would be the use of 2D nanomaterials, such as graphene as an electrode material and surface coating. Graphene has previously been used as the anode material of an MFC with a pure culture of *E. coli* and delivered a maximum power density of 2668 mW/m^2, which was 17 to 18 times larger than the stainless-steel mesh and poly-tetrafluoroethylene modified electrodes, respectively (Zhang et al., 2011). However, it can cause high operating cost which may not make it feasible to use for general uses.

In this current work, a parametric study is carried out to find the effect of the variation of anodic and cathodic materials in terms of voltage generation in Microbial Fuel Cell. Three different types of materials (Copper, Graphite and Zinc) are selected as the construction material of anode and cathode and then the parametric variation is

observed for the combination of each cathodic material for three types of anodes. Significant amount of voltage generation was witnessed in each of nine different types of MFC setup. To validate the experimental results, a Pseudo two dimensional (2D) full cell mathematical model was developed. Mathematical model is validated through experimental results. Detail of this study will provide more insight information.

EXPERIMENTAL SETUP AND METHODS

Construction of microbial fuel cell

For the experiment, total six MFCs systems were made. To minimize the cost of membrane, two chamber MFC was built. Figure 1 indicates the schematic diagram of dual chamber microbial fuel cell. Each of the cells consisted of same water sample but different types of cathode and anode materials. It needs to make sure that the electrodes are conductive, does not react with the solution and are biocompatible (Logan et al., 2006) Copper, zinc and graphite are chosen as to prepare the electrodes. The weights of the electrodes were measured using a digital weight machine (MEGA KING, Model: AS-CA). Graphite, zinc and copper electrodes were used in the form of cylindrical bar with surface area of 55.08 cm^2.

Physical characteristics of the materials

The volume of wastewater in each MFC was 5 L. The characteristic of wastewater is shown in Table 1. The volume of surface water was also 5 L. The room temperature was 32°C. Bacteria in the anode side are influenced with changing room temperature and the volume of waste-water in the anode chamber (Liu and Cheema, 2012). Each chamber was made of plastic material (Polypropylene (PP)/HDPE). The chamber, containing waste-water was anodic chamber and an electrode was dipped into it. The anodic chamber was air sealed so that oxygen from environment cannot pass into it. The cathode chamber, containing surface water was exposed to air and another electrode was dipped into it. A U-tube made of glass was used to connect both chambers. A solution of Potassium Chloride (KCL) and Agar-Agar powder was made for the salt bridge. Both electrodes were connected through external wire. A multi-meter was used to monitor the Open Circuit Voltage (OCV) of the system. The system was observed for 30 h.

Working procedure

Wastewater consists of numerous amounts of bacteria and organic materials. Microorganisms respire using these organic materials for living. They leave electrons to an electron acceptor, that is, oxygen during respiration. However, wastewater has a high biochemical oxygen demand (BOD) and low dissolved oxygen (DO). So oxygen is collect from the air. But the anode compartment, containing wastewater is airtight. For this reason, the microorganisms cannot collect oxygen for respiration. Microorganisms in the anode compartment form biofilms on the anode surfaces with, considering it as an electron acceptor oxidizes organic compounds that are present in the wastewater (Min and Logan, 2004; Dumas et al., 2008). These generated electrons are transferred to cathode by an external wire and combines with electron acceptor (oxygen) (Rahimnejad et al., 2015). Figure 2 illustrates the working procedure of an MFC. By this method a voltage difference is found between the chambers. The electricity is then extracted from the external wire. This voltage is measured by a multi-meter (DT9205A Digital Multi-meter). The main organic substrate in wastewater is Glucose ($C_6H_{12}O_6$). The oxidation reduction reactions in a MFC are (Gude 2015) oxidation reaction (Anode)

$$C_6H_{12}O_6 + 12H_2O \rightarrow 6HCO_3^- + 30H^+ + 24e^- \quad (1)$$

Reduction reactions (Cathode):

$$O_2 + 4H^+ + 4e^- \rightarrow 2H_2O \quad (2)$$

Overall reaction:

$$C_6H_{12}O_6 + 6H_2O \rightarrow 6CO_2 + 24H^+ + 24e^- \quad (3)$$

According to various published studies, the cathodic reaction may be the most noteworthy factor to affect the performance of MFCs (Zeng et al., 2010). As time goes on, the number of bacteria in anode chamber keeps decreasing as there is no oxygen. Because of these the voltage difference between the two chambers also decreases. The more the number of bacteria in the sample, the better the reading of voltage of the cell.

MFC cycling test

MFC setup has been made with 6 different combinations such as Graphite-Zinc, Graphite-Copper, Copper-Copper, Copper-Zinc, Zinc-Zinc, and Zinc-Copper. Next, all the 6 types of cells were inspected for 10 h. After that, maximum voltage of all the 6 types of cells was identified. During this observation, voltage and current were measured by multi-meters. Then, Current and Power densities were calculated by following equation:

$$P = VI \quad (4)$$

Next to check the voltage generation capability in a particular time period, we generated Voltage (mV) vs Time (h), Current (mA) vs Time (h), Voltage (V) vs Current Density (mA/m^2) Graph. Then, to check the ability of power generation in each cell, Power Density (mW/m^2) vs Current Density (mA/m^2) graph for all combinations.

Development of numerical models

To check the voltage storage capacity in MFC setup, a mathematical model is developed here likewise (Valoen and Reimers, 2005). Mathematical model for lithium-ion batteries (LIBs) prepared. It was observed that MFC setups generated similar number of voltages like LIBs. Therefore a mathematical model was developed which is similar to the LIB mathematical model (Valoen and Reimers, 2005). LIBs usually consist of current collector, positive electrode, separator, and negative electrode. An organic solution fills the porous components and serves as electrolyte (Figure 3). Since our model is a two-dimensional (2D) full-cell model, the model developed in this study assumed the particles to be a two-phase system. A porous electrode model that reflects this schematic was developed to estimate the reaction distribution across the electrode. The governing equations and boundary conditions (Table 2) for this model have been discussed in the literature. These equations are composed of mass conservation in the solid phases, mass conservation in electrolyte phase, conservation of charge in solid phase, conservation of charge in electrolyte phase, Butler-Volmer (BV) equation associated to describe the electrochemical reaction at the interface.

Mass conservation in solid phase

To estimate diffusion coefficients in the particle using data, Fick's

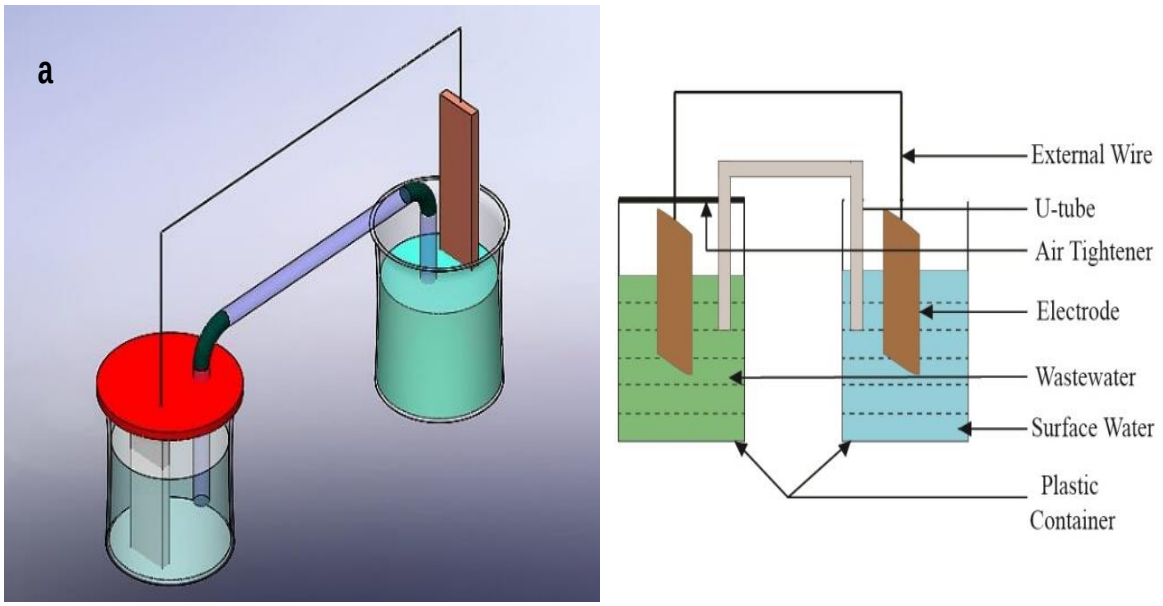

Figure 1. (a) Schematic diagram of the experimental setup of Microbial Fuel Cell (MFC); (b) 2D diagram of different components of the experimental setup of Microbial Fuel Cell (MFC) (Hossain et al., 2020; Masud et al., 2021).
Source: Author's 2022

Table 1. Physical characteristics of wastewater (Miah et al., 2017; Tariquzzaman et al., 2016).

Wastewater specification	Value	Unit
BOD	100	mg O_2/L
Turbidity	101	FTU
E. coli	2400	CFU/100 ml
pH	6.9	-

Source: Author's 2022

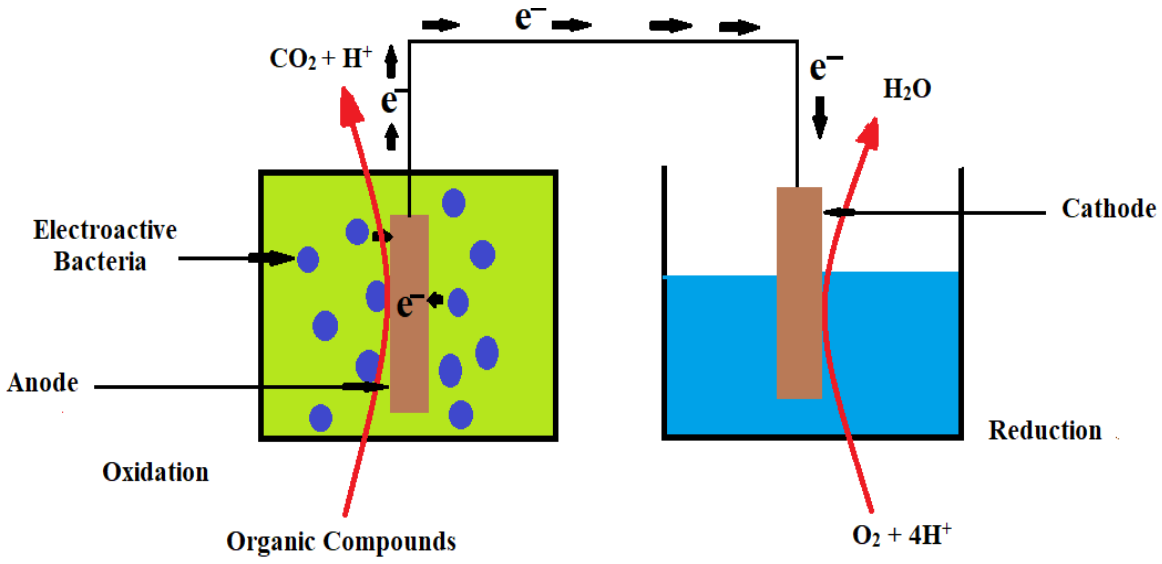

Figure 2. Schematic of a microbial electrolysis cell. (Hossain et al., 2022, Masud et al., 2021)
Source: Author's 2022

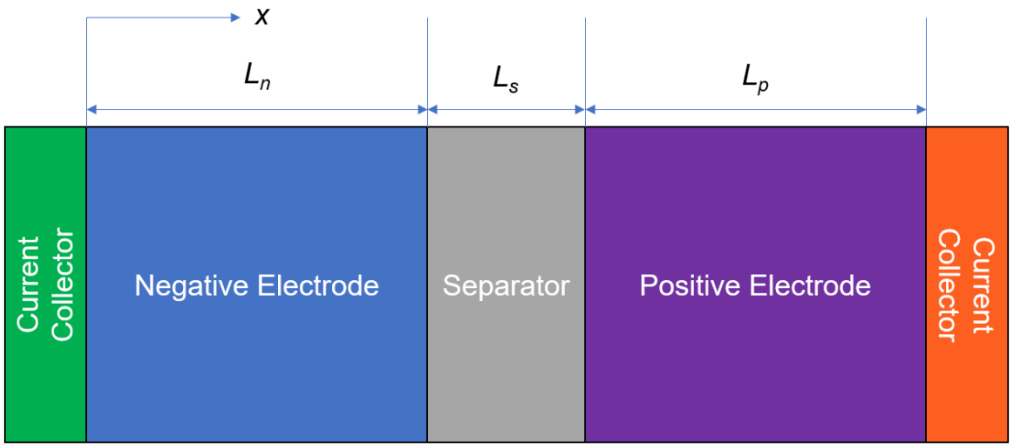

Figure 3. Schematic of a microbial fuel cell setup.
Source: Author's 2022

Table 2. Governing equations and boundary conditions for porous electrode (half-cell) model.

Governing equations	Boundary conditions
Mass conservation in solid phase (spherical coordinate) $\frac{\partial C_{s,i}}{\partial t} = \frac{D_s}{r^2}\frac{\partial}{\partial r}\left(r^2\frac{\partial C_{s,i}}{\partial r}\right)$	$\left.\frac{\partial C_{s,i}}{\partial r}\right\|_{r=0} = 0, -D_s\left.\frac{\partial C_s}{\partial r}\right\|_{r=r_0} = \frac{i_i}{F}$
Mass conservation in electrolyte phase $\varepsilon_i\frac{\partial C_{e,i}}{\partial t} = \frac{\partial}{\partial x}\left(D_{eff,i}\frac{\partial C_{e,i}}{\partial x}\right) + (1-t_+^0)a_i J_i$	$-D_{eff,p}\left.\frac{\partial C_{e,p}}{\partial x}\right\|_{x=0} = -D_{eff,n}\left.\frac{\partial C_{e,n}}{\partial x}\right\|_{x=L_p+L_s+L_n} = 0$
Conservation of charge in solid phase $\sigma_{eff,i}\frac{\partial^2 \emptyset_{s,i}}{\partial x^2} = a_i F J_i$	$\sigma_{eff,p}\left.\frac{\partial \emptyset_{s,p}}{\partial x}\right\|_{x=0} = I_{app}, \sigma_{eff,n}\left.\frac{\partial \emptyset_{s,n}}{\partial x}\right\|_{x=L_p+L_s+L_n} = 0$
Conservation of charge in electrolyte phase $\frac{\partial}{\partial x}\left(\kappa_{eff,i}\frac{\partial \emptyset_{e,i}}{\partial x}\right) + \frac{2RT\kappa_{eff,i}}{F}\frac{\partial}{\partial x}\left(\frac{\partial \ln c_e}{\partial x}\right) = -a_i F J_i$	$-\kappa_{eff,p}\left.\frac{\partial \emptyset_{e,p}}{\partial x}\right\|_{x=0} = -\kappa_{eff,p}\left.\frac{\partial \emptyset_{e,n}}{\partial x}\right\|_{x=L_p+L_s+L_n} = 0$
Butler-volmer kinetic equation $J_i = k_i(C_{s,max} - C_{s,surf})^{\alpha} C_e^{1-\alpha}\left\{\exp\left[\frac{\alpha F}{RT}(\emptyset_s - \emptyset_e - U)\right] - \exp\left[-\frac{(1-\alpha)F}{RT}(\emptyset_s - \emptyset_e - U)\right]\right\}$	
Effective properties $\kappa_{eff} = \kappa\varepsilon_e^{\gamma}$ $D_{eff} = D_e\varepsilon_e^{\gamma}$ $\sigma_{eff,i} = \varepsilon_s\sigma$	Specific interfacial surface area $a_i = \frac{3\varepsilon_s}{r_0}$ Diffusion coefficient in electrolyte phase $D_e = 10^{-4}\times 10^{-4.43-\left(\frac{54}{T-229-5.0\times10^{-3}c_i}\right)-0.22\times10^{-3}c_i}$ Ionic conductivity in electrolyte phase $\kappa_{i,e} = 10^{-4}\times c_i(-10.5 + 0.688\times10^{-3}c_i + 0.494\times10^{-6}c_i^2 + 0.074T - 1.78\times10^{-5}c_iT - 8.86\times10^{-10}c_i^2T - 6.96\times10^{-5}T^2 + 2.80\times10^{-8}c_iT^2)^2$

Source: Author's 2022

law (Equation 5) was numerically solved in spherical coordinates (Valoen and Reimers, 2005).

$$\frac{\partial c_{s,i}}{\partial t} = D_{s,i}\frac{\partial^2 c_{s,i}}{\partial r^2} + 2\frac{D_{s,i}}{r}\frac{\partial c_{s,i}}{\partial r} \quad (5)$$

where $i = p$ is considered for the positive electrode and $i = n$ is chosen for negative electrode. The boundary and initial conditions are

$$D\frac{\partial c_{s,i}}{\partial r} = -\frac{i_{app}}{a_i LF} \quad \text{for} \quad r = r_0 \quad (6)$$

$$D\frac{\partial c_{s,i}}{\partial r} = 0 \quad \text{for} \quad r = 0 \quad (7)$$

In Equation 7, the right-side value is zero as at the center of the particle, the flux value is zero. whereas in Equation 6, on the surface of the particle, the flux value is equivalent to the consuming/producing rate of ions due to the electrochemical reaction occurring at the solid/liquid interphase.

$$c_{s,0} = c_0 \quad \text{for} \quad t = 0 \quad (8)$$

where r_0 is the particle radius, c_s is the ion concentration, $c_{s,0}$ is the initial ion concentration, D_s is the diffusion coefficient, i_{app} is the current density, a_i is the surface-to-volume ratio, L is cell thickness, F is the Faraday's constant. In estimating the diffusion coefficients, both particle volume changes and stress effects were ignored.

Mass conservation in electrolyte phase

The mass conservation for the binary electrolyte in the liquid phase is described by:

$$\varepsilon_i\frac{\partial c_{e,i}}{\partial t} = \frac{\partial}{\partial x}\left(D_{eff,i}\frac{\partial c_{e,i}}{\partial x}\right) + \frac{(1-t_+^0)i_{app}}{LF} \quad (9)$$

Here, $i = p, s$ and n. In the separator the pore wall flux is equal to zero. ε_i is defined emissivity. t_+^0 is exhibited as Transference number. c_e is the concentration of the electrolyte. At the two ends of the cell in the x-direction, there is no mass flux, that is,

$$-D_{eff,p}\frac{\partial C_{e,p}}{\partial x}\Big|_{x=0} = 0 \quad (10)$$

$$-D_{eff,n}\frac{\partial C_{e,n}}{\partial x}\Big|_{x=L_n+L_s+L_p} = 0 \quad (11)$$

At the interfaces between positive electrode/separator and separator/negative electrode, the concentration of the binary electrolyte and its flux are continuous. The effective diffusion coefficient, $D_{eff,i}$ of the binary electrolyte in the liquid phase is corrected by porosity (Valoen and Reimers, 2005),

$$D_{eff,i} = D_{e,i}\varepsilon_i^{\gamma} \quad (12)$$

where the diffusion coefficient of the binary electrolyte, $D_{e,i}$ can be expressed as follows:

$$D_{e,i} = 10^{-4}x10^{-4.33-\left(\frac{54}{T-229-5.0x10^{-3}c_i}\right)-0.22x10^{-3}c_i} \quad (13)$$

Here, T is denoted as the Temperature. c_i is defined as concentration of solid/electrolyte.

Conservation of charge in solid phase

The charge balance in the solid phase is governed by Ohm's law,

$$\sigma_{eff,i}\frac{\partial^2 \emptyset_{s,i}}{\partial x^2} = \frac{i_{app}}{L} \quad (14)$$

Here $i = p$ and n. The effective conductivity is determined by $\sigma_{eff,i} = \sigma_i\varepsilon_i^{\gamma}$. The specific area can be calculated by $a_i = \frac{3\varepsilon_i}{r_{s,i}}$. At the interface of current collector and positive electrode, the charge flux is equivalent to current density applied to the cell,

$$\sigma_{eff,n}\frac{\partial \emptyset_{s,p}}{\partial x}\Big|_{x=0} = I_{app} \quad (15)$$

$$\sigma_{eff,p}\frac{\partial \emptyset_{s,n}}{\partial x}\Big|_{x=L_n+L_s+L_p} = 0 \quad (16)$$

The potential of the solid phase at the right end of the cell is equal to 0. $\emptyset_{s,n}|_{x=L_p+L_s+L_n} = 0$, and potential of the solid phase at $x=0$, $\emptyset_{s,p}|_{x=0}$ is equal to E_{cell} (the cell voltage).

Conservation of charge in electrolyte phase

The conservation of charge in electrolyte phase is based on Ohm's law is given by:

$$\frac{\partial}{\partial x}\left(\kappa_{eff,i}\frac{\partial \emptyset_{e,i}}{\partial x}\right) + \frac{2RT\kappa_{eff,i}}{F}\frac{\partial}{\partial x}\left(\frac{\partial \ln c_e}{\partial x}\right) = -\frac{i_{app}}{L} \quad (17)$$

Here, $i = p,s$ and n and the specific conductivity of the binary electrolyte, $\kappa_{eff,i}$ is a function of temperature and the concentration of the binary electrolyte in the liquid phase (Valoen and Reimers, 2005).

$$\kappa_{eff,i} = \kappa_i\varepsilon_i^{\gamma} \quad (18)$$

where the expression of the ionic conductivity for the binary electrolyte is given as:

$$\kappa_i = 10^{-4}xc_i(-10.5 + 0.668x10^{-3}c_i + 0.494x10^{-6}c_i^2 + 0.074T - 1.78x10^{-5}c_iT - 8.86x10^{-10}c_i^2 - 6.96x10^{-5}T^2 + 2.80x10^{-8}c_iT^2)^2 \quad (19)$$

At the two ends of the cell, no charge flux in the liquid phase is found,

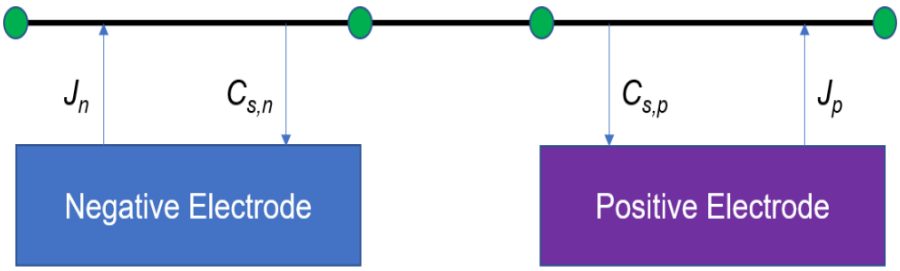

Figure 4. Geometries and variables coupling between used in COMSOL Multiphysics.
Source: Author's 2022

$$-\kappa_{eff,n}\left.\frac{\partial \emptyset_{e,p}}{\partial x}\right|_{x=0} = 0 \quad (20)$$

$$-\kappa_{eff,n}\left.\frac{\partial \emptyset_{e,n}}{\partial x}\right|_{x=L_n+L_s+L_p} = 0 \quad (21)$$

The potential in the solution phase and its flux are continuous at the interfaces of the electrodes and the separator. In this model, the wall flux, j_i is determined by Butler-Volmer (BV) equation. BV equation can be expressed:

$$j_i = \frac{i_0}{F}\left\{\exp\left[\frac{F(V-U)-\phi_s-\phi_e}{2RT}\right] - \exp\left[-\frac{F(V-U)-\phi_s-\phi_e}{2RT}\right]\right\} \quad (22)$$

j_i is net flux, mol/m^2/s. Is defined as:

$$j_i = \frac{i_{app}}{a_i VLF} \quad (23)$$

Therefore, Equation 7 can be expressed as follows:

$$\frac{i_{app}}{a_i VLF} = \frac{i_0}{F}\left\{\exp\left[(1-\alpha)\frac{F(V-U)-\phi_s-\phi_e}{RT}\right] - \exp\left[-\alpha\frac{F(V-U)-\phi_s-\phi_e}{RT}\right]\right\} \quad (24)$$

where α is the symmetric coefficient, i_0 is the exchange current density, R is the universal gas constant, T is the temperature. If we use α= 0.5, Equation 21 can be written as:

$$V = U + \phi_s + \phi_e + \frac{2RT}{F}\sinh^{-1}\left(\frac{i_{app}}{2i_0 a_i VLF}\right) \quad (25)$$

where V is the applied voltage, U is the open-circuit potential, ϕ_s is the potential in solid phase, ϕ_e is the potential in electrolyte phase. The exchange current density equation can be represented as:

$$i_0 = F k_0 c_e^{1-\alpha}(c_{max} - c_s)^{1-\alpha} c_s^{\alpha} \quad \textbf{(26)}$$

Here, F is Faraday's constant. k_0 is rate constant, c_{max} is the maximum concentration, and c_s is the solid concentration.

Solution procedure

The mathematical model equations were solved using a finite-element package COMSOL Multiphysics 5.6. Model parameters such as electrode design, thermodynamics, transport, kinetic, and mechanical properties are listed in Table 1.

Mathematical model is a multi-scale model. Several geometries are developed including 1D geometry which consists of three sequentially connected lines to represent positive electrode, separator, negative electrode, respectively, a two-dimensional (2D) geometry which consists of two rectangles to define solid phase in electrodes.

The geometries are as shown in Figure 4. The vertical co-ordinate in the two-dimensional geometry denotes the radial direction of the solid particles. Since the diffusion of ions in the x-direction in the particle is ignored, the corresponding diffusion coefficient is set to zero in this direction. The concentration of the binary electrolyte, the potential in the electrolyte, the potential in the solid phase and the wall flux are solved in the one-dimensional geometry. The concentration of ions in the solid phase is solved in the 2D geometry. The wall flux is extruded from the 1D domain and projected to the top boundary of the 2D geometry by using "linear extrusion coupling" in COMSOL Multi-physics. The concentration of ions on the top boundary in the 2D geometry is projected to the 1D domain by using "boundary extrusion coupling". The cell is charged for 10 h at C/10. The validity of the parameter choice is checked by comparing the physics model to experiments, as shown in Table 3.

RESULTS AND DISCUSSION

Here, MFC setups are made of six different anodic-cathode combinations such as Graphite-Zinc (Gr-Zn), Graphite-Copper (Gr-Cu), Copper-Zinc (Cu-Zn), Copper-Copper (Cu-Cu), Zinc-Zinc (Zn-Zn) and Zinc-Copper (Zn-Cu). All the experimental setups are kept idle and monitored for 10 h and self-voltage generation and current generation are witnessed. Next, from the experimental data, Voltage vs Time, Current vs Time, Voltage vs Current Density, and Power Density vs Current Density curves are generated. Then by using our developed mathematical model all these four types of curves are produced. Model generated curves are then used to validate experimental results. By comparing experimental results with simulation results best suited MFC setup is identified which has the potential to be next generation energy storage device.

In Figure 5, Voltage (mV) vs Time (h) curves are generated. The red dotted line denotes model generated curves. Whereas the other coloured dashed lines

Table 3. List of model parameters used in this study.

Symbol	Units	Cathode	Separator	Anode	Reference
Area of the cell, A	m^2		55.0E-4		Hossain, 2020; Hossain et al., 2020
Thickness, L	m	116E-6	100E-6	116E-6	Hossain, 2020, 2021; Hossain et al., 2020; Hossain and Kim, 2020
Particle radius, r_0	m	5E-7	-	5E-7	Hossain, 2020
Active particle volume fraction, ε_i		0.6517	-	0.6517	Hossain, 2020; Hossain et al., 2020
Electrolyte phase volume fraction, ε_e		0.417	0.50	0.417	Hossain, 2020; Hossain et al., 2020
Initial molar concentration, c_0	mol/m^3		$x_0 X c_{max}$		Hossain, 2020
Concentration in electrolyte, c_e	mol/m^3		1000		Hossain, 2020; Hossain et al., 2020
Max solid phase concentration, $c_{max,i}$	mol/m^3		ρ×*Capa*/*F*		Hossain, 2020, 2021; Hossain et al., 2020; Hossain and Kim, 2020
Reaction rate coefficient, $\alpha_{a,I}$, $\alpha_{c,I}$		0.5	-	0.5	Hossain et al., 2020; Hossain and Kim, 2020
Bruggeman constant, γ		1.5	1.5	1.5	Hossain and Kim, 2020
Li-ion diffusion coefficient in solid phase, D_s	m/s^2	2.0E-16	-	2.0E-16	Hossain, 2020; Hossain et al., 2020
Solid phase conductivity, κ_i	S/m	0.1	-	1	Hossain, 2020; Hossain et al., 2020
Conductivity of solid matrix, σ_{eff}	S/m		10		Hossain et al., 2020; Hossain and Kim, 2020, Haque and Rahaman (2021)
Reaction rate constant, k_i	mol/m/s		5.0E-11		Hossain, 2020; Hossain et al., 2020
Cationic transport number, t^+		0.4	1.0	0.4	Hossain et al., 2020; Hossain and Kim, 2020
Faraday's constant, F	C/mol	96485.33			Hossain, 2020; Hossain et al., 2020
Universal gas constant, R	J/mol/k	8.31416			Hossain, 2020; Hossain et al., 2020
Ambient temperature, T	K	298.15			Hossain, 2020, 2021; Hossain et al., 2020; Hossain and Kim, 2020; Ojeda et al., 2022
Density, ρ	kg/m^3	2500			Hossain, 2020, 2021; Hossain et al., 2020; Ojeda et al., 2022

Source: Author's 2022

symbolize voltage curves generated by experimental setups. After 10 h of observation, mathematical model generated 1040.750 (mV). On the other hand, Gr-Zn experimental MFC setup produced 1060.012 (mV) and Gr-Cu combination generated 1005.038 mV in 10 h. During same time-period Cu-Zn produced 974.100 mV, meanwhile Cu-Cu, Zn-Zn and Zn-Cu generated 920.116, 675.121 and 607.205 mV of voltage, respectively. From Figure 5 it seen in comparison with simulation results, Gr-Zn, Gr-Cu setups are most productive cells in terms of voltage generation. In Figure 5, it is seen as time progresses, voltage increases. This phenomenon indicates that all the MFC setups have self-voltage generation capability.

Figure 6 displays current (mA) vs time (h) curves. Likewise, Figure 5, red coloured lines show mathematical model generated curves. Whereas other coloured dashed lines show experimental data. It is seen, when time is 0, the initial current is in maximum limit and after 10 h current reaches 0 values. In terms of mathematical model generated curves, maximum current is found as 82.500 mA. Whereas, for the experimental setups of Gr-Zn, Gr-Cu, Cu-Zn, Cu-Cu, Zn-Zn, and Zn-Cu maximum current values are figured out as 82.359, 82.309, 82.240, 82.199, 82.174, and 81.139 mA, respectively. From Figure 6, it was noted that current decreases as the time progresses in all the cells including mathematical model generated results. As reported in (Rahimnejad et al., 2015; Cai and White, 2011; Hossain et al., 2020), in a MFC cell, if current keeps decreasing voltage generation keeps increasing. After 10 h, the current reaches minimum limit and cell generates maximum amount of voltage.

Here, in Figure 7 Voltage (mV) vs Current Density (mA/m^2) curves are generated for both experimental MFC setups and mathematical model. Current density is calculated by dividing current with cross-sectional area of the anodic cell. From Figure 7, the red dotted line denotes experimental data whereas the coloured dashed lines show experimental setups' generated data. The simulated results show when current density is at 0 mA/m^2, voltage remains maximum at 1040.750 mV whereas when current density reaches 15.000 mA/m^2, voltage drops down to 0 mV. The mathematical model generated a straight slope curve which is closed to an

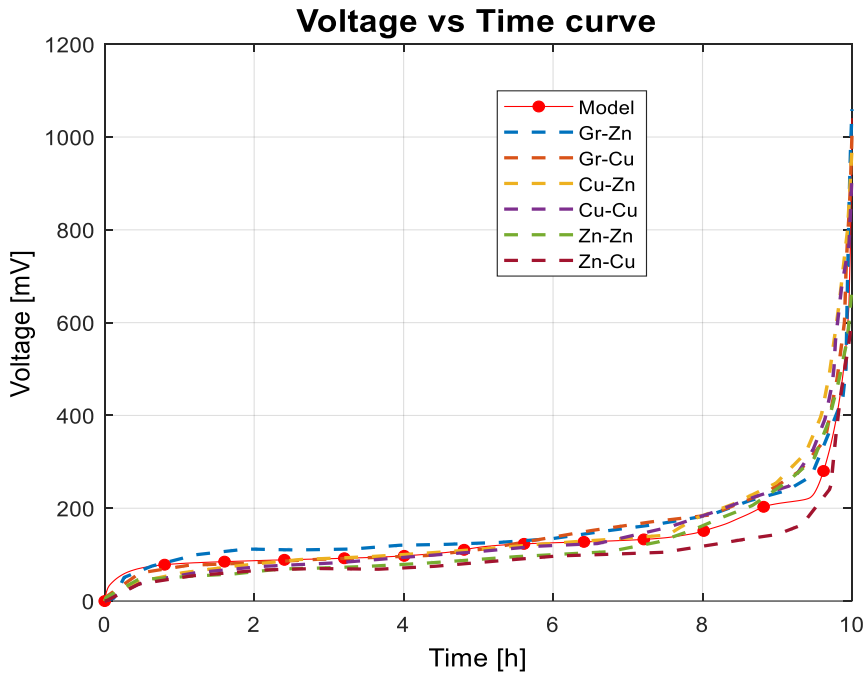

Figure 5. Voltage (mV) vs Time (h) curves.
Source: Author's 2022

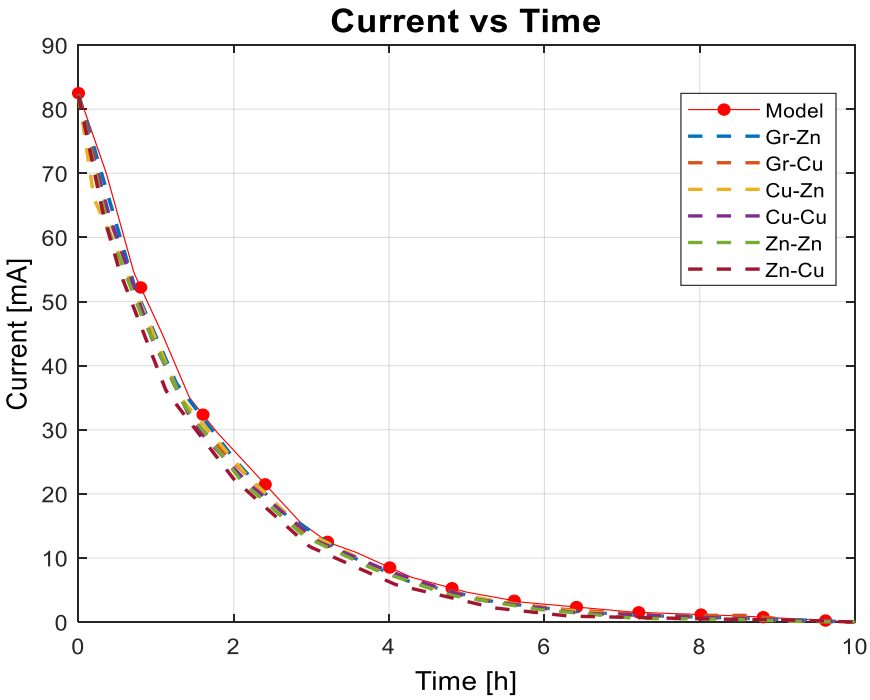

Figure 6. Current (mA) vs Time (h) curves.
Source: Author's 2022

ideal curve. Next, other experimental voltage vs current density curves are witnessed to find which MFC setups are closed to mathematical model. It was observed that Gr-Zn and Gr-Cu curves are close to model generated curve, whereas Zn-Zn and Zn-Cu experimental curves are far from ideal model curve.

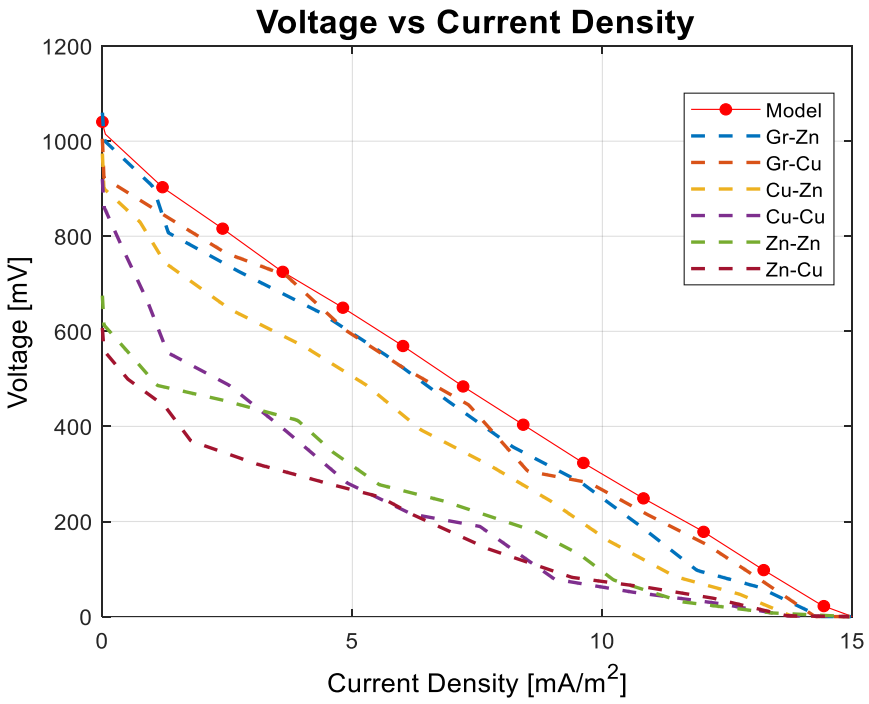

Figure 7. Voltage (mV) vs Current Density (mA/m^2) curves.
Source: Author's 2022

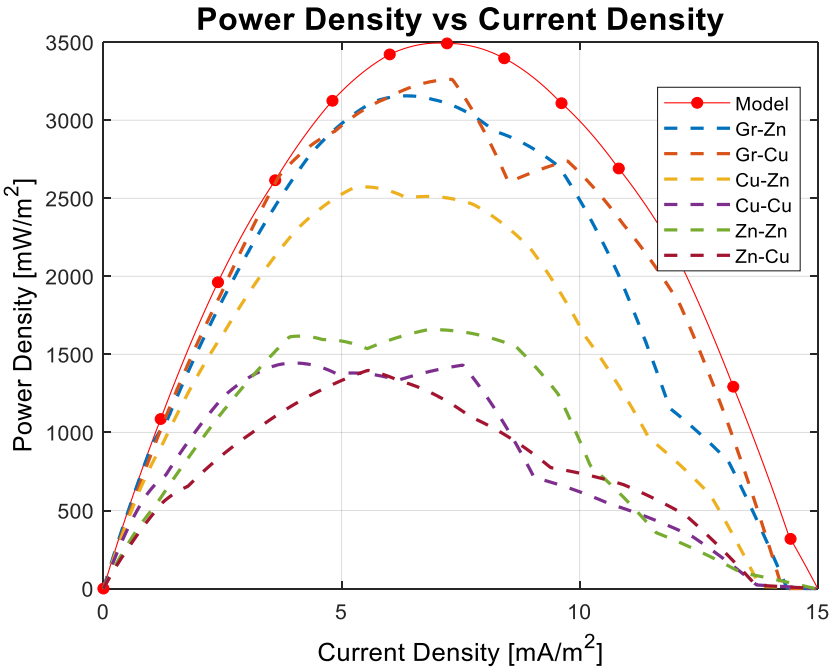

Figure 8. Power Density (mW/m^2) vs Current Density (mA/m^2) curves.
Source: Author's 2022

Figure 8 shows Power Density (mW/m^2) vs Current Density (mA/m^2) curves generated by different experimental setups and mathematical model. Power density is calculated by multiplying voltage with current

density. In Figure 8, red dotted lines show mathematical model generated curve and the dashed coloured lines denote experimental setup generated curves. It is to be noticed from model generated curve, at the initial stage both power and current density remain 0. As the current density progresses power density keeps increasing. At the half-way stage when current density's value is 7.501 mA/m^2, power density reaches maximum limit of 3500.001 mW/m^2. After that point power density again keeps decreasing and when current density reaches maximum limit of 15.000 mA/m^2, power density again drops down to 0. These model generated line makes a parabola curve. Similarly, with the experimental data, power density vs current density curves are generated with all the six experimental setups. Mathematical model generated curve is used to validate experimental results. It can be noted that, Gr-Zn and Gr-Cu curves' shapes are very close to mathematical model generated curve shape, whereas Cu-Zn, Cu-Cu, Zn-Zn and Zn-Cu curves do not match with model generated curve.

From the experimental and simulation results of Voltage vs Time, Current vs Time, Voltage vs Current Density, and Power Density vs Current Density curve, the mathematical model generated curves of a perfect MFC cell model. It was noticed from Figures 5 and 6, experimental results of all six different cells generated similar results of mathematical model. Whereas, from Figures 7 and 8, among all the setups Gr-Zn (dashed blue line) produced closest results to MFC model, then Gr-Cu (dashed brown line) generated results are found to be the second closest to MFC model. On the other hand, Cu-Zn (dashed yellow line), Cu-Cu (dashed violet line), Zn-Zn (green dashed line), and Zn-Cu (maroon dashed line) produced results which is far from the ideal model.

The mathematical model, in MFC setup development for anode the material properties of graphite have been used, whereas for cathode, the same for lithium was used. The MFC model behaves very close to LIB model. Alternatively in Gr-Zn MFC setup, graphite has been used as anode, whereas Zinc has been used as cathode. For Gr-Cu setup, graphite has been used as anode and Cu has been used as cathode. It is to be noted from the comparison of mathematical model and experimental setup, if1 MFC can be made with Graphite anode and Zn cathode, it will generate maximum amount of voltage in a specific time and the setup can be used as the next generation energy storage device. The next best MFC setup can be chosen as the one made of graphite anode and copper cathode. The rest of the setups do not have enough voltage generation capacity and their energy density is too low to be considered as an energy storage device.

Conclusion

In this work, the voltage generation capacity of small-scale MFC is thoroughly investigated. The microbial fuel cells are made of various anode-cathode combination setups. Then, voltage, current and power density curves are generated with experimental data. After that, a pseudo 2D model has been developed with the entire ideal parameters and graphs are obtained with mathematical model showing close comparability with experimental results. Among all these combination, experimental voltage and power density curves generated from Graphite-Zinc setup match the best with ones generated from mathematical model. The ideal model produces maximum amount of voltage as using Butler-Volmer Voltage equation is with key parameters. The Graphite-Copper setup also produced closest result to ideal fuel cell model. Here, these two cells have the capability to produce significant amounts of voltages (Approx. 1.0 V) which can be found in the commercial Lithium-Ion batteries. Whereas the other combinations of electrode materials do not have capability to produce enough voltages as they have lower energy density and significantly low electrical voltage production rate when electrodes are submerged in an electrolyte solution. The power density curves generated from both experiment and simulation also suggests that Graphite-Zinc MFC combo is the best one which is close to LIBs in terms of performance followed by Graphite-Copper setup. From this observation it can be said that Graphite-Zinc and Graphite-Copper MFC has significant voltage generation capacity and can be used as an alternate economical medium of energy storage device commercially in the future.

CONFLICT OF INTERESTS

The authors have not declared any conflict of interests.

REFERENCES

Belleville P, Strong P, Dare P, Gapes D (2011). Influence of nitrogen limitation on performance of a microbial fuel cell. Water Science and Technology 63(8):1752-1757.

Cai L, White R (2011). Mathematical modelling of a lithium-ion battery with thermal effects in COMSOL Inc. Multiphysics (MP) software. Journal of Power Sources, 196(14):5985-5989.

Chaudhuri S, Lovley D (2003). Electricity generation by direct oxidation of glucose in mediatorless microbial fuel cells. Nature Biotechnology 21(10):1229-1232.

Chen, C, Chen T, Chung Y (2013). A comparison of bioelectricity in microbial fuel cells with aerobic and anaerobic anodes. Environmental Technology, 35(3):286-293.

Cœuret F, Vilar E, Cavalcanti E (2002). Carbon fibre cloth as an electrode material: electrical conductivity and mass transfer . Journal of Applied Electrochemistry 32(10):1175-1182.

Dumas C, Mollica A, Féron D, Basseguy R, Etcheverry L, Bergel A (2008). Checking graphite and stainless anodes with an experimental model of marine microbial fuel cell. Bioresource Technology 99(18):8887-8894.

Ghasemi M, Daud W, Hassan S, Oh S, Ismail M, Rahimnejad M, Jahim J (2013). Nano-structured carbon as electrode material in microbial fuel cells: A comprehensive review. Journal of Alloys and Compounds 580:245-255.

Gude V (2016). Wastewater treatment in microbial fuel cells – an

overview. Journal of Cleaner Production 122:287-307.
Haque E, Rahaman M (2021). First-principles prediction of structural stability and thermoelectric properties of SrGaSnH. RSC Advances 11:3304-3314
Hernández-Flores G, Poggi-Varaldo HM, Solorza-Feria O, Ponce Noyola MT, Romero-Castañón T, Rinderknecht-Seijas N (2015). Tafel Equation Based Model for the Performance of a Microbial Fuel Cell. International Journal of Hydrogen Energy 40(48):17421-17432.
Hossain A (2020). Development of a physics-based mathematical model of microparticle silicon based lithium half cells. Available at: http://www.dissertations.wsu.edu/Thesis/Fall2020/A_Hossain_121420.pdf (Accessed on October 12:2022
Hossain A (2021). Development of a Mathematical Model to Study the Impact of State of Charge Dependent Exchange Current Density on the Generated Voltage Hysteresis of Silicon Anode-based Lithium Half Cells. Journal of Mechanical Engineering Research 12(1):37-48.
Hossain A, Cha Y, Song M, Kim S (2020). Side Reaction Correction and Non-linear Exchange Current Density for Mathematical Modelling of Silicon Anode Based Lithium-Ion Batteries. Available at: https://www.vancouver.wsu.edu/research-showcase/research-showcase-gallery-poster-2207 (Accessed on June 15, 2022)
Hossain A, Kim S (2020). Development of a physics-based mathematical model to analyse the limitations of microparticle silicon-based lithium half cells. IMECE Technical Presentation. Available at: https://www.researchgate.net/publication/346031457_Development_of_a_Physics-Based_Mathematical_Model_to_Analyze_the_Limitations_of_Microparticle_Silicon_Based_Lithium_Half_Cells_IMECE_Technical_Presentation (Accessed on June 15, 2022)
Hossain A, Masud N, Yasin M, Ali M (2020). Analysis of the Performance of Microbial Fuel Cell as a Potential Energy Storage Device. Proceedings of International Exchange and Innovation Conference on Engineering and Sciences 6(6):149-155.
Hossain A, Masud N, Ali M (2022). Comprehensive cost analysis of electrochemical performance in microbial fuel cells. Microbial Fuel Cells: Emerging Trends in Electrochemical Applications 1:350
Li F, Sharma Y, Lei Y, Li B, Zhou Q (2009). Microbial Fuel Cells: The Effects of Configurations, Electrolyte Solutions, and Electrode Materials on Power Generation. Applied Biochemistry and Biotechnology 160(1):168-181.
Liu H, Logan B (2004). Electricity Generation Using an Air-Cathode Single Chamber Microbial Fuel Cell in the Presence and Absence of a Proton Exchange Membrane. Environmental Science and Technology 38(14):4040-4046.
Liu J, Qiao Y, Guo C, Lim S, Song H, Li C (2012). Graphene/carbon cloth anode for high-performance mediator-less microbial fuel cells. Bioresource Technology 114: 275-280.
Liu X, and Cheema I (2012). Managing Process Streams at Sjölunda WWTP with Electricity- Producing Bacteria Investigation of Alkalinity Redistribution and Maximum Current Generation Capacity in Bio electrochemical Systems. Department of Chemical Engineering, Lund University, Sweden.
Logan B, Regan J (2006). Microbial Fuel Cells—Challenges and Applications. Environmental Science & Technology, 40(17):5172-5180.
Logan B, Hamelers B, Rozendal R, Schröder U, Keller J, Freguia S, Aelterman P, Verstraete W, and Rabaey K (2006). Microbial Fuel Cells: Methodology and Technology. Environmental Science and Technology, 40 (17):5181-5192.
Lu Z, Chang D, Ma J, Huang G, Cai L, and Zhang L (2015). Behavior of metal ions in bioelectrochemical systems: A review. Journal of Power Sources 275:243-260.
Masud N, Hossain A, Moresalein M, Ali M (2021). Performance Evaluation of Microbial Fuel Cell with Food Waste Solution as a Potential Energy Storage Medium. Proceedings of International Exchange and Innovation Conference on Engineering and Sciences 7:96-102.
Miah M, Majumder A, and Latifa G (2017). Evaluation of microbial quality of the surface water of Hatirjheel in Dhaka City. Stamford Journal of Microbiology 6(1):30-33.
Min B, Logan B (2004). Continuous Electricity Generation from Domestic Wastewater and Organic Substrates in a Flat Plate Microbial Fuel Cell. Environmental Science and Technology 38(21):5809-5814.
Min B, Cheng S, Logan B (2005). "Electricity generation using membrane and salt bridge microbial fuel cells. Water Research 39(9):1675-1686.
Oh S, Logan B (2005). Hydrogen and electricity production from a food processing wastewater using fermentation and microbial fuel cell technologies. Water Research 39(19):4673-4682.
Ojeda B, Waliullah M, Hossain A, Nguyen T, Wettstein T, Tadesse Y, Bernal R (2022). High-throughput tensile testing of silver nanowires (2022). Extreme Mechanics Letters 56:101896
Oliveira V, Simões M., Melo L, Pinto A (2013). A 1D mathematical model for a microbial fuel cell. Energy 61:463-471.
Pinto R, Srinivasan B, Manuel M, Tartakovsky B (2010). A two-population bio-electrochemical model of a microbial fuel cell. Bioresource Technology 101(14):5256-5265.
Rahimnejad M, Adhami A, Darvari S, Zirepour A, Oh S (2015). Microbial fuel cell as new technology for bioelectricity generation: A review. Alexandria Engineering Journal 54(3):745-756.
Rosenberg B, Van Camp L, and Krigas T (1965). Inhibition of Cell Division in Escherichia coli by Electrolysis Products from a Platinum Electrode. Nature, 205(4972):698-699.
Tariquzzaman S, Nishu S, Saeed T, Ahmed R (2016). Water Quality and EIA of Simple Hatirjheel Lake. Conference: Proceedings of the 3rd International Conference on Civil Engineering for Sustainable Development (ICCESD).
Valdez-Vazquez I, Ríos-Leal E, Carmona-Martínez A, Muñoz-Páez K, Poggi-Varaldo H (2006). Improvement of Biohydrogen Production from Solid Wastes by Intermittent Venting and Gas Flushing of Batch Reactors Headspace. Environmental Science and Technology 40(10):3409-3415.
Valoen L, Reimers J (2005). Transport Properties of LiPF6 -Based Li-Ion Battery Electrolytes. Journal of the Electrochemical Society 152(5):A882-892.
Walter X, Forbes S, Greenman J, Ieropoulos I (2016). From single MFC to cascade configuration: The relationship between size, hydraulic retention time and power density. Sustainable Energy Technologies and Assessments 14:74-79.
Wei J, Liang P, Huang X (2011). Recent progress in electrodes for microbial fuel cells. Bioresource Technology, 102(20):9335-9344.
Yang C (2009). An impending platinum crisis and its implications for the future of the automobile. Energy Policy 37(5):1805-1808.
Zeng Y, Choo Y, Kim B, Wu P (2010). Modelling and simulation of two-chamber microbial fuel cell. Journal of Power Sources 195(1):79-89.
Zhang Y, Mo G, Li X, Zhang W, Zhang J, Ye J, Huang X, Yu C (2011). A graphene modified anode to improve the performance of microbial fuel cells. Journal of Power Sources 196(13):5402-5407.

APPENDIX

List of symbols	
Applied current density [A]	I_{app}
Cell thickness [m]	L
Diffusion coefficient [m^2/s]	$D_{s,i}$
Effective conductivity	σ_i
Effective conservation of charge in electrolyte phase	$\kappa_{eff,i}$
Effective conservation of charge in solid phase	$\sigma_{eff,i}$
Effective diffusion coefficient [m^2/s]	$D_{eff,i}$
Effective diffusion coefficient of binary electrolyte [m^2/s]	$D_{e,i}$
Emissivity of Ion	ε_i
Exchange current density [A/m^2]	i_0
Faraday's constant [C/mol]	F
Initial concentration of electrolyte [mol/m^3]	$C_{e,i}$
Initial lithium concentration [mol/m^3]	$c_{s,0}$
Initial particle radius [m]	r_0
Ionic conductivity for binary electrolyte	κ_i
Molar concentration [mol/m^3]	$c_{s,i}$
Net flux [mol/m^2s]	j_i
Potential in electrolyte phase [V]	ϕ_e
Potential in solid phase [V]	ϕ_s
Rate of charging/discharging	C_{Rate}
Rate constant	k_0
Surface-to-volume ratio	$a_i V$
Symmetric coefficient	α
Temperature [K]	T
Transference number	t_+^0
Universal gas constant [J/mol/k]	R